Exploration of Catalytic Properties of CYP2D6 and CYP3A4 Through Metabolic Studies of Levorphanol and Levallorphan⟨S⟩

Britta Bonn, Collen M. Masimirembwa, and Neal Castagnoli, Jr.

Department of Chemistry, Medicinal Chemistry, University of Gothenburg, Gothenburg, Sweden (B.B.); Discovery DMPK, AstraZeneca Research and Development, Mölndal, Sweden (B.B., C.M.M.); African Institute of Biomedical Science and Technology, Harare, Zimbabwe (C.M.M.); and Department of Chemistry, Virginia Tech and the Edward Via College of Osteopathic Medicine, Blacksburg, Virginia (N.C.)

ABSTRACT:

CYP2D6 and CYP3A4, two members of the cytochrome P450 superfamily of monooxygenases, mediate the biotransformation of a variety of xenobiotics. The two enzymes differ in substrate specificity and size and characteristics of the active site cavity. The aim of this study was to determine whether the catalytic properties of these isoforms, reflected by the differences observed from crystal structures and homology models, could be confirmed with experimental data. Detailed metabolite identification, reversible inhibition, and time-dependent inhibition were examined for levorphanol and levallorphan with CYP2D6 and CYP3A4. The studies were designed to provide a comparison of the orientations of substrates, the catalytic sites of the two enzymes, and the subsequent outcomes on metabolism and inhibition. The metabolite identification revealed that CYP3A4 catalyzed the formation of a variety of metabolites as a result of presenting different parts of the substrates to the heme. CYP2D6 was a poorer catalyst that led to a more limited number of metabolites that were interpreted in terms to two orientations of the substrates. The inhibition studies showed evidence for strong reversible inhibition of CYP2D6 but not for CYP3A4. Levallorphan acted as a time-dependent inhibitor on CYP3A4, indicating a productive binding mode with this enzyme not observed with CYP2D6 that presumably resulted from close interactions of the N-allyl moiety oriented toward the heme. All the results are in agreement with the large and flexible active site of CYP3A4 and the more restricted active site of CYP2D6.

CYP3A4 and CYP2D6 are two members of the cytochrome P450 (P450) superfamily of monooxygenases that catalyze the biotransformation of a variety of xenobiotics (Guengerich, 2003). CYP3A4 has a large, flexible active site (Ekroos and Sjögren, 2006) resulting in broad substrate selectivity. CYP2D6 is more substrate-selective because of its smaller active site and the presence of specific amino acid residues that may contribute to substrate-enzyme interactions (Koymans et al., 1992; de Groot et al., 1997; Lewis et al., 1997).

To gain further structural information of the P450s, efforts have been directed toward the crystallization of these enzymes. The crystallization of soluble bacterial P450s (Poulos et al., 1987) provided an opportunity to conduct homology modeling studies of human P450s using these bacterial crystal structures as templates (Lewis, 1999; De Rienzo et al., 2000). The crystallizations of human CYP3A4 in 2004 (Williams et al., 2004; Yano et al., 2004) and CYP2D6 in 2006 (Rowland et al., 2006) allow for an extension of homology modeling to include direct comparisons with the human enzymes. A comparison of crystal structures and homology models has been published re-

cently (Kjellander et al., 2007). This comparison involved docking solutions of a set of compounds for which specific interactions with the surrounding amino acid residues had been identified by computational methods. In addition, the opportunity to predict sites of metabolism for the different structures was investigated. The compound class used for this study was a family of morphinanyl opioid analgesics. These compounds are known substrates for both CYP2D6 and CYP3A4 that presumably adopt different orientations in the active sites of the two isoforms (Kirkwood et al., 1997; Yue and Sawe, 1997; von Moltke et al., 1998; Benetton et al., 2004; Hutchinson et al., 2004). CYP3A4 preferentially catalyzes the oxidative N-demethylation, and CYP2D6 catalyzes the oxidative O-demethylation of selected members of this class of compounds. Attempts to dock some of these probe molecules into the active sites of CYP3A4 as defined by its X-ray crystal structure led to ambiguous results. The large and flexible active site cavity of this enzyme resulted in orientations with different parts of the molecules in close proximity to the heme. This in turn led to a variety of solutions for the predicted sites of metabolism. Because the experimentally determined sites of metabolism reported in the article by Kjellander et al. (2007) considered major metabolic pathways only, a more detailed characterization of the metabolic profiles of two compounds of the series has been pursued. The experimental results were expected to provide information about

ABBREVIATIONS: P450, cytochrome P450; TDI, time-dependent inhibition; AMMC, 4-aminomethyl-7-methoxycoumarine; BFC, 7-benzyloxy-4-trifluoromethylcoumarine; HPLC, high-performance liquid chromatography; MS, mass spectrometry; XIC, extracted ion chromatogram; TIC, total ion current chromatogram; NR, normalized ratio; Cl_{int}, intrinsic clearance.
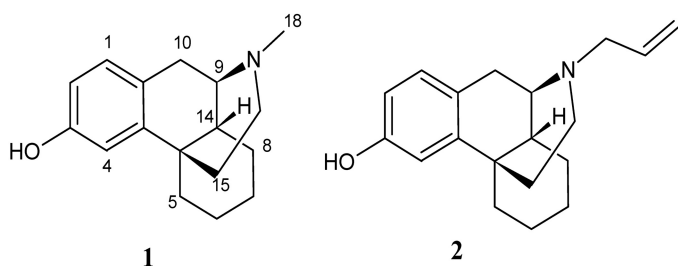
FIG. 1. Structures of levorphanol (**1**) and levallorphan (**2**).

the different orientations the molecules adopt in CYP2D6 and CYP3A4 as part of an effort to characterize further the differences between the two isoforms, regarding interactions and active site cavities, observed with computational methods.

The two compounds selected for this study (Fig. 1) were levorphanol (**1**) and levallorphan (**2**). Levorphanol, an *N*-methylmorphinanyl derivative, serves as the prototype for this family of opioid analgesics. The second compound, levallorphan (**2**), was selected because of the presence of the *N*-allyl side chain that might be involved in hydrophobic interactions in the active site cavity that could result in an improved affinity. Furthermore, compounds bearing the allylaminyl group present in levallorphan have been reported to undergo metabolic activation leading to time-dependent inhibition (TDI) of the enzyme (Fontana et al., 2005). Consequently, the TDI properties of levorphanol and levallorphan were compared using the two enzymes. In addition, the reversible inhibition potential was determined for the compounds as a measure of the affinity for the two P450 isoforms. It was anticipated that these results would give further information on the productive orientations of these two molecules in the active sites of CYP3A4 and CYP2D6. Also included in this article are dockings of the two compounds based on the crystal structures of CYP3A4 and CYP2D6.

Materials and Methods

Materials. The recombinant enzymes used in these studies (human P450s CYP2D6 and CYP3A4 coexpressed with NADPH-P450 reductase in bacterial membranes) were supplied from Cypex Ltd. (Dundee, Scotland, UK). Levorphanol tartrate, levallorphan tartrate, NADPH, and GSH were purchased from Sigma-Aldrich (St. Louis, MO), and 4-aminomethyl-7-methoxycoumarine (AMMC) and 7-benzyloxy-4-trifluoromethylcoumarine (BFC) were from BD Gentest (Woburn, MA). Propranolol and troleandomycin were supplied from Sigma-Aldrich. HO-Bufuralol, bufuralol, and 1′-HO-midazolam were purchased from SAFC Corp. (St. Louis, MO), and midazolam was from Lipomed AG (Arlesheim, Switzerland). All of the other chemicals were of analytical grade and of the highest quality available.

Bioanalytical Equipment and Analytical Methods. High-performance liquid chromatography/mass spectrometry (HPLC/MS) and HPLC/MS^2 were conducted for the metabolite identification studies. The HPLC system was an Agilent 1100 Series (Hewlett-Packard GmbH, Waldbronn, Germany) coupled to an HTC PAL autosampler (CTC Analytics AG, Zwingen, Switzerland). The analytical column used for chromatographic separation of the metabolites was a HyPURITY C$_{18}$ column (100 × 2.5 mm, 5 μm; Thermo Fisher Scientific, Waltham, MA). The mobile phases consisted of 0.1% formic acid in water (A) and 0.1% formic acid in acetonitrile (B). The gradient was increased linearly from 5% solvent B to 50% solvent B in 8 min at a flow rate of 0.75 ml/min. The HPLC system was connected to a Sciex API 4000 quadrupole mass spectrometer with electrospray ionization interface (Applied Biosystems, Concord, ON, Canada). Positive ion mass spectra were recorded over the mass range *m/z* 80 to 400, followed by product ion scans on peaks of interest. The collision energy used was 40 eV. The Analyst 1.4.1 software (Applied Biosystems) was used for analysis and storage of data.

Additional MS^2 experiments using a Waters (Wythenshawe, Manchester, UK) quadrupole time-of-flight Premiere instrument were performed to obtain accurate mass data. The MS^2 analyses were performed on the metabolites

observed on the Sciex API 4000 quadrupole mass spectrometer (Applied Biosystems). The collision energy was ramped from 20 to 40 eV, and the cone voltage was set to 35 V. For chromatographic separation, a Waters (Milford, MA) ACQUITY UPLC was used with a Waters ACQUITY UPLC C$_{18}$ column (50 × 2.1 mm, 1.18 μm). The same mobile phases as on the Agilent 1100 series instrument (Hewlett-Packard GmbH) were used. The gradient of 5 to 90% B was achieved in 5 min; the flow rate was 0.75 ml/min. MassLynx version 1.4 software (Waters) was used for analysis and storage of data.

The analysis of HO-bufuralol and 1′-HO-midazolam for the IC$_{50}$ determinations was performed with HPLC/MS on the Sciex API 4000 instrument (Applied Biosystems) described above. The multiple reaction monitoring transitions used were 2778.1/185.7 for HO-bufuralol and 342.0/202.7 for HO-midazolam. The column used for chromatographic separation was a HyPURITY C$_{18}$ column (50 × 2.5 mm, 5 μm; Thermo Fisher Scientific).

Metabolite Identification in Incubations with Recombinant Enzymes. The metabolic profiles of levorphanol (**1**) and levallorphan (**2**) were investigated with recombinant CYP2D6 and CYP3A4. The compounds (10 μM) were mixed with enzyme (100 pmol/ml) and phosphate buffer (0.1 M, pH 7.4). Each mixture was preincubated for 10 min at 37°C, and the reaction was then initiated by addition of NADPH (1 mM). Zero time samples were taken before the addition of NADPH. After 60 min, the incubations were quenched with the addition of an equal amount of ice-cooled solution of 0.8% formic acid in acetonitrile. The samples were centrifuged, and the supernatant was diluted 1:1 in water before analysis. The 0- and 60-min samples were used for identification of metabolites.

In the case of levallorphan (**2**), incubations were also performed in the presence of GSH to capture any reactive species. The same incubation conditions as above were used with the addition of GSH (5 mM).

To quantify the turnover of the parent compound, intrinsic clearance (Cl$_{int}$) values for levorphanol and levallorphan were determined at 1 μM. The compounds were mixed with recombinant P450 (50 pmol/ml) and potassium phosphate buffer (0.1 M, pH 7.4). After 10-min preincubation, the reaction was initiated by addition of NADPH (1 mM), and the incubations were continued for 7, 15, 20, and 30 min. Zero time point samples were taken just before addition of NADPH. All the incubations were performed in microtiter plates at 37°C. The reaction was quenched with two parts ice-cooled acetonitrile containing 0.8% formic acid. The samples were centrifuged at 2737*g* for 20 min at 4°C, and the supernatant was diluted 1:2 with water before analysis.

IC$_{50}$ Determination. For determination of the potential of the test compounds to inhibit reversibly CYP2D6 and CYP3A4, full IC$_{50}$ curves were obtained with recombinant P450s. The inhibition of the catalytic activity of the enzymes was studied using bufuralol and midazolam as probe substrates for CYP2D6 and CYP3A4, respectively. Serial dilutions of the test compounds were done in 50% acetonitrile (50.00, 16.70, 5.50, 1.90, 0.60, 0.20, 0.07, and 0.02 μM). These solutions were added to a master mix containing enzyme (5 pmol/ml), potassium phosphate buffer (0.2 M, pH 7.4), and the probe substrates bufuralol (10 μM) for CYP2D6 and midazolam (3 μM) for CYP3A4. Also included were blank samples, without test compound and substrate, and incubations containing only the substrate (100% activity). The incubation mixtures were preincubated for 10 min, and the reactions were initiated by addition of NADPH (1 mM), except for the blank samples. After incubating for 15 min, the reactions were quenched with ice-cooled acetonitrile containing 0.8% formic acid. All the incubations were performed in microtiter plates at 37°C. The plates were centrifuged at 2737*g* for 20 min at 4°C, and the supernatants were diluted 1:2 in water before analysis. The CYP2D6 samples were diluted again 1:10. Standard curves of 1′-HO-midazolam and HO-bufuralol were prepared in the incubation matrix and were precipitated in the same way as the samples. The formation of 1′-HO-midazolam and HO-bufuralol were analyzed with HPLC/MS.

Time-Dependent Inhibition. Levorphanol and levallorphan were tested for their TDI properties. A time-dependent inhibitor is a compound that inhibits the enzyme in an irreversible or quasi-irreversible manner after metabolic activation. In this assay the activities of recombinant CYP2D6 and CYP3A4 were measured with the fluorescent probe substrates AMMC and BFC after 0, 5, 10, and 20 min of preincubation with the test compound. For the determination of the extent of enzyme inactivation, the enzymes were incubated at 37°C with the test compound (1.5, 12.5, and 25 μM) in the presence and

absence of NADPH (1 mM for CYP3A4 and 0.4 mM for CYP2D6). Control incubations were included without any test compound present. After preincubation, a 20-μl aliquot of the preincubation mixture was transferred to a well containing BFC (50 μM) or AMMC (60 μM), NADPH (1 mM for CYP3A4 and 0.4 mM for CYP2D6), and phosphate buffer (0.2 M) at a final volume of 200 μl. To decrease the impact of reversible inhibition, substrate concentrations at 4$\times$ K_m were used to saturate the enzyme. A 1/20 dilution of the preincubation mixture into the incubation with substrate was also tested to further rule out a reversible inhibition component. The final protein concentration was 1.25 pmol/ml CYP3A4 and 20 pmol/ml CYP2D6. The higher enzyme concentration with CYP2D6 was used to obtain a sufficient signal-to-noise ratio when measuring the fluorescence of the AMMC metabolite. The incubations were quenched after 15 min with a stop solution containing 80% acetonitrile and 20% Tris. The catalytic activities were determined from the amount of metabolite formed from the probe substrates by measuring the fluorescence at 390/460 nm for AMMC and at 405/535 nm for BFC. This was done using a SpectraMax Gemini XS fluorescence detector (Molecular Devices, Sunnyvale, CA). The percentage of remaining activity was calculated by dividing the counts in the samples with the counts in the control incubations (100% activity). Included in the assays were positive controls known to act as time-dependent inhibitors on the two enzymes. These were propranolol for CYP2D6 (Narimatsu et al., 2001) and troleandomycin for CYP3A4 (Yamazaki and Shimada, 1998).

Dockings of Levorphanol and Levallorphan into Crystal Structures of CYP2D6 and CYP3A4. Dockings of levorphanol and levallorphan in CYP2D6 and CYP3A4 were performed to visualize possible orientations in the active site cavities. The protein structures used were the ligand-free CYP2D6 crystal structure (Protein Data Bank code 2f9q) (Rowland et al., 2006), and the CYP3A4 crystal structure cocrystallized with erythromycin (Protein Data Bank code 2j0d) (Ekroos and Sjögren, 2006). In the study by Kjellander et al. (2007), these two crystal structures were evaluated regarding site of metabolism predictions of compounds in the same family as levallorphan and levorphanol. Consequently, these structures were chosen for the purpose of this study. The CYP2D6 crystal structure has some unresolved regions; however, these are assumed not to affect the environment of the active site. Because the aim was to visualize possible orientations of the compounds, settings were used to restrict the dockings based on knowledge of the two enzyme active site cavities. The substrates were drawn in ISISdraw (Symyx Technologies Inc.,

Sunnyvale, CA) and exported as sdf-files. The two- to three-dimensional conversion was made with CORINA (Molecular Networks GmbH, Erlangen, Germany; http://www.mol-net.de). For the dockings in CYP2D6 substrate molecules were protonated because the electrostatic interactions are believed to be important for the orientation in the CYP2D6 active site cavity. As in the study by Kjellander et al. (2007), neutral molecules were used for the dockings in CYP3A4.

The dockings were performed with the docking module GLUE in program GRID version 22.2.2 (Molecular Discovery, Pinner, Middlesex, UK; http://moldiscovery.com). This program is based on calculations of GRID-molecular interaction fields (Goodford, 1985). Specific probes related to the two compounds studied were chosen for analysis of the active site of the enzyme. In CYP2D6 these were H (hydrogen), OH2 (water), DRY (hydrophobic), N1+ (sp^3 aminyl cation), C3 (methyl), C1 = (sp^2 CH aromatic or vinylic), and OH (phenol or carboxyl). For CYP3A4 the same probes were used except for N1+, which was exchanged for N: (sp^3 N with a lone pair). For the analysis a distance of 1 Å between the grid points was used. To restrict the dockings, a box estimated to include the heme and active site was used ($\sim$16 $\times$ 20 $\times$ 23 Å). In the dockings possible interactions with surrounding water molecules were not considered. For the binding affinity estimation, contributions from electrostatic interactions were included, as well as a penalty for loss of rotatable torsions. Different conformations of the ligands were generated in GLUE using random search by rotating a maximum of five rotatable bonds. A maximum number of binding sites was set to 100, and an energy cutoff to -100 kcal/mol was included. Because the aim was to provide possible productive binding modes, the resulting docking poses were filtered, and only those that were within 6 Å from any atom of the heme were selected for further analysis.

Results

Identification of Levorphanol Metabolites. An analysis of the product ion spectrum (Fig. 2) of protonated levorphanol (**1H$^+$**) was undertaken to provide comparative data that would be useful in the elucidation of the structures of metabolites derived from this compound. This spectrum (as well as the corresponding spectra of levallorphan and the derived metabolites) could be obtained only at a high collision dissociation energy (40 eV) because of the stability of
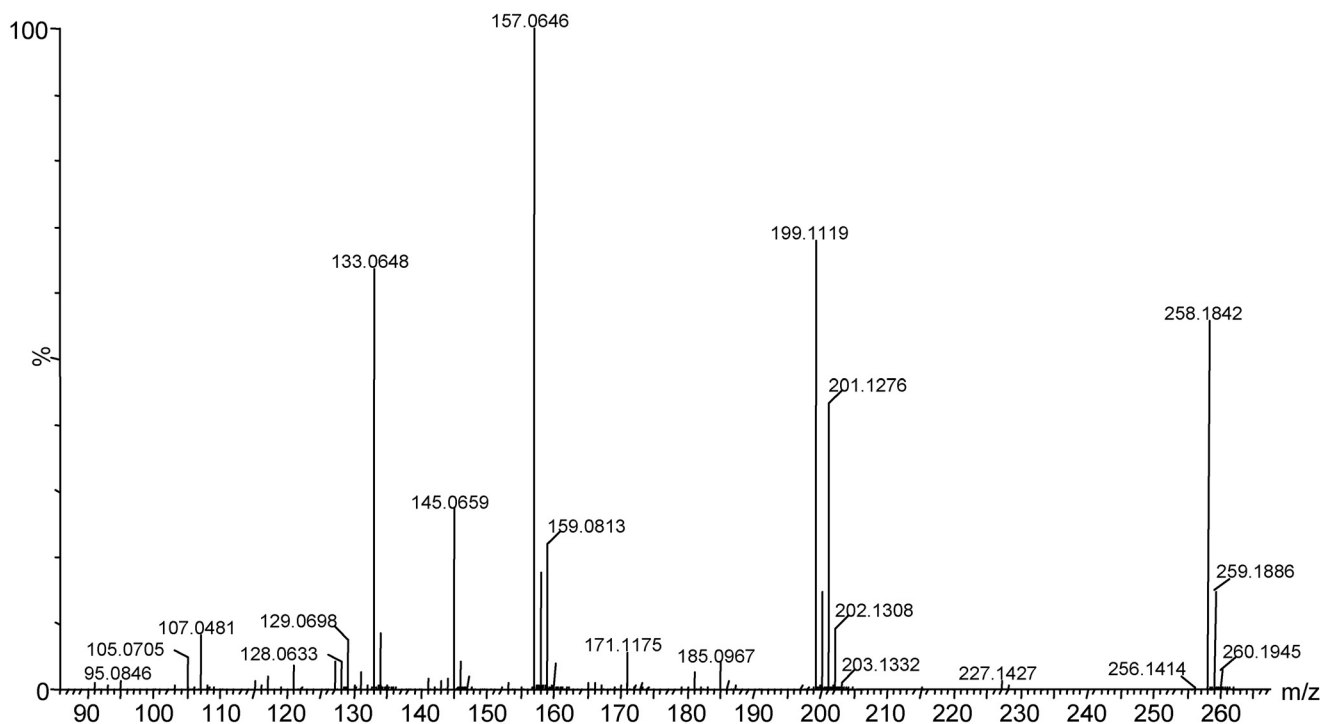

FIG. 2. HPLC/electrospray ionization/MS product ion spectrum of protonated levorphanol (**1H$^+$**) obtained at 40 eV.

the **MH$^+$** species. The molecular formulas for the major product ions were obtained from accurate mass analysis (Table 1). Structure assignments and attempts to rationalize the formation of the major product ions are detailed in the supplemental data.

Two informative product ions present in this spectrum, at m/z 201.1277 (C$_{14}$H$_{17}$O$^+$) and 199.1120 (C$_{14}$H$_{15}$O$^+$), are likely to correspond to **ii$^+$** and **iii$^+$**, respectively. Pathways to rationalize the formation of these product ions (Scheme 1) start with ring-opening and proton rearrangements of **1H$^+$**. Migration of a proton from the *N*-methyl group to C(9) with simultaneous ring opening leads to **1a$^+$** that loses ethene and formaldimine to yield **ii$^+$** [path (a)]. Alternatively, cleavage of the C(9)-N bond accompanied by proton migration from the benzylic C(10) atom to nitrogen leads to **ib$^+$**. Subsequent fragmentation with neutral losses of ethene and methylamine leads to **iii$^+$** [path (b)]. The product ions observed in this spectrum are also present in the product ion spectrum of protonated levallorphan (see below). Furthermore, the corresponding spectra obtained from several

metabolites of levorphanol and levallorphan display product ions equivalent to **ii$^+$** and **iii$^+$**.

Levorphanol Metabolites Formed in the Presence of CYP3A4 and CYP2D6. The extracted ion chromatograms (XICs) obtained from incubations of levorphanol with CYP3A4 and CYP2D6 of all the metabolite peaks are shown in Fig. 3. (See supplemental data for all the total ion current chromatograms.) The product ions are recorded in Table 2. Peaks corresponding to six metabolites (**3-8**) were observed in the XICs for CYP3A4, and three of these metabolites (**4**, **6**, and **8**) were formed in the presence of CYP2D6. The m/z for MH$^+$ of **3**, **4**, and **5** (m/z 274) was 16 m/z units greater than **1H$^+$** (m/z 258); the m/z for MH$^+$ of **6** (m/z 244) was 14 m/z units less than that of **1H$^+$**; and the m/z for MH$^+$ of **7** and **8** (m/z 260) was 2 m/z units greater than **1H$^+$**. The suggested metabolic pathways of levorphanol with CYP3A4 and CYP2D6 are summarized in Scheme 2.

Based on the principal product ions, the structure of the ion with MH$^+$ at m/z 274.1799 is assigned to the C(8)-hydroxylated species **3** (Scheme 2). The product ion present at m/z 256.1709, corresponding to loss of water, supports an aliphatic, as opposed to aromatic, site of hydroxylation. The proposed position of the hydroxylation at C(8) is based on the structures of the product ions at m/z 215.1067 (**xii$^+$**), 173.0596 (**xiii$^+$**), and 157.0659 (**v$^+$** via **xi$^+$**) (see Supplemental Data Scheme S2 for details).

The m/z values of the ions observed in the product ion spectrum of the compound assigned the structure **4H$^+$** correspond to those observed in the product ion spectrum of **1H$^+$** with the addition of 16 m/z units. The structure of this metabolite is suggested to be a dihydroxyphenyl species (**4** in Scheme 2, unknown regiochemistry) because the product ion spectrum shows no loss of water. Proposed structures of the other product ions are consistent with this assignment (see Supplemental Data Scheme S3).

TABLE 1

Comparison of calculated and experimentally determined masses for the product ions observed in the product ion spectrum of protonated levorphanol (1H$^+$)

Product Ion[a]	Found Mass	Suggested Formula	Exact Mass	Difference (ppm)
ia$^+$ and **ib$^+$**	258.1842	C$_{17}$H$_{24}$NO$^+$	258.1858	6.2
ii$^+$	201.1277	C$_{14}$H$_{17}$O$^+$	201.1279	1.0
iii$^+$	199.1120	C$_{14}$H$_{15}$O$^+$	199.1123	1.5
iv$^+$	159.0813	C$_{11}$H$_{11}$O$^+$	159.0810[a]	1.9
v$^+$	157.0646	C$_{11}$H$_9$O$^+$	157.0653[a]	4.5
vii$^+$	145.0659	C$_{10}$H$_9$O$^+$	145.0653[a]	4.1
ix$^+$	133.0647	C$_9$H$_9$O$^+$	133.0653[a]	4.5

[a] Proposed structures and fragmentation pathways to rationalize product ions with these formulas will be found in the supplemental data.
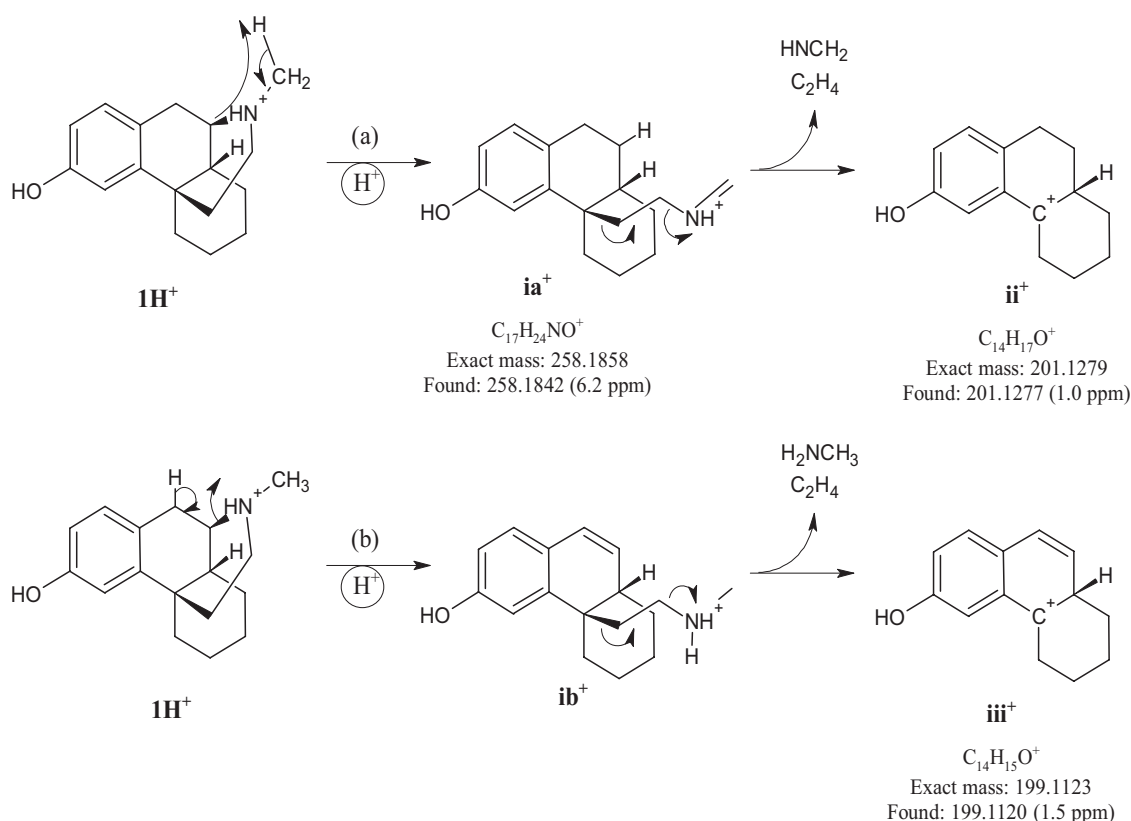
SCHEME 1. Pathways proposed to account for the product ions at m/z 201.1277 (**ii$^+$**) and 199.1120 (**iii$^+$**).

The product ion spectrum of the third metabolite assigned with MH$^+$ 274.1793 shows the same ions as observed with $\mathbf{1H^+}$ together with two additional ions at m/z 257.1777 and m/z 256.1703. The ion at m/z 256.1703, corresponding to loss of water, is consistent with a second aliphatic hydroxylation product. However, the ion at m/z 257.1777 corresponds to a loss of 17 m/z units from the parent. The only reasonable assignment for a neutral loss of 17 m/z units from this system is the hydroxyl radical (·OH). Loss of ·OH suggests that the oxidation of $\mathbf{1}$ has taken place on a position that can fragment to give a relatively stable radical cation. Therefore, the suggested structure of this metabolite is the N-oxide ($\mathbf{5}$ in Scheme 2) (see Supplemental Data Scheme S4 for details). This assignment is supported by the longer

retention time of this metabolite compared with that of the parent. Both $\mathbf{3}$ and $\mathbf{5}$ may be unresolved diastereomeric mixtures.

The metabolite with MH$^+$ at m/z 244.1696 is a compound with 14 m/z units less than that of protonated levorphanol ($\mathbf{1H^+}$). This loss of 14 m/z units corresponds to loss of a methylene group and suggests that the structure of this metabolite is the secondary amine ($\mathbf{6}$ in Scheme 2). This proposal is supported by the observed product ions (Table 2) that correspond to those found in the product ion spectrum of $\mathbf{1H^+}$ and all of which involve pathways (a) and (b) outlined in Scheme 1.

The remaining two metabolites have an MH$^+$ at m/z 260.1636, 2 m/z units greater than that of $\mathbf{1H^+}$. Based on the proposed structures of $\mathbf{3}$, $\mathbf{4}$, and $\mathbf{6}$, these metabolites are likely to result from
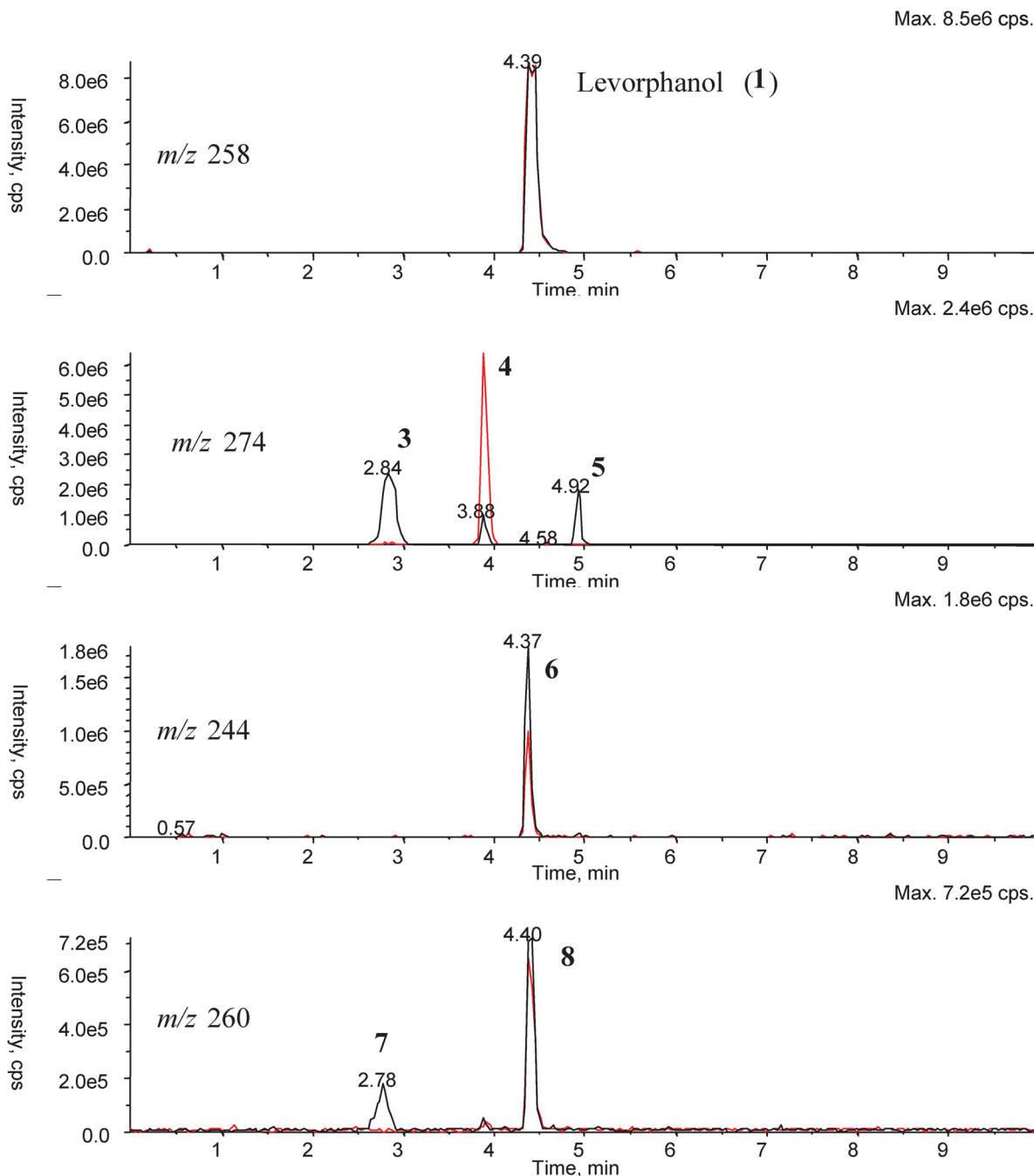

FIG. 3. XICs obtained from extracts of incubation mixtures of levorphanol (10 μM) in the presence of NADPH-supplemented recombinant CYP3A4 (black) and CYP2D6 (red).

TABLE 2

Molecular mass, responsible P450, and MH⁺-generated product ions of levorphanol (1), levallorphan (2), and their metabolites

| Compound	P450	MH⁺ at m/z	Product Ions >10% Relative Abundance
Levorphanol (1)		258	201, 199, 159, 157,[a] 145, 133
3	3A4	274	256, 215, 199, 197, 173, 157,[a] 145
4	3A4/2D6	274	217, 215, 175, 173,[a] 161, 149
5	3A4	274	257, 256, 201, 199, 159, 157,[a] 145, 133
6	3A4/2D6	244	201, 199, 159, 157,[a] 145, 133
7	3A4	260	242, 215, 199, 173, 157,[a] 145
8	3A4/2D6	260	202, 200, 158,[a] 157, 134, 133
Levallorphan (2)		284	201, 199, 159, 157,[a] 145, 133
6	3A4/2D6	244	201, 199, 159, 157,[a] 145, 133
9	3A4	300	282, 215, 199, 197, 173, 157,[a] 145
10	3A4/2D6	300	217, 215, 175, 173,[a] 161, 149
11	3A4/2D6	316	298, 231, 215,[a] 213, 189, 173, 161
12	3A4	316	231, 215, 213, 197,[a] 169
13	3A4	258	215, 187, 159, 146, 145,[a] 133, 107

[a] Base peak.

a combination of *N*-demethylation (−14 *m/z* units) and hydroxylation (+16 *m/z* units). The product ions formed from the protonated **7** species resemble those observed from **3H⁺**, suggesting that this is the *N*-demethylated metabolite of **3** (**7** in Scheme 2). The product ions at *m/z* 242.1613 (loss of water), 215.1097 (losses of ethene and methylamine), and 173.0591 (subsequent loss of cyclopropane) are consistent with structure **7**. The product ion spectrum of the second species with MH⁺ at *m/z* 260 was very weak. Because there is no evidence for loss of water in the spectrum, this compound may be the *N*-demethylated dihydroxyphenyl species **8** (Scheme 2).

Because no authentic standards were available, only approximate estimates of the quantities of the metabolites formed, from integrated ion intensities, were possible. Even if this is not a proper way of quantification it gives an opportunity to compare the distribution of metabolites for the compound studied. The MS response area and a calculation of the relative MS area (%MS) of all the metabolites and the parent are presented in Table 3. CYP3A4 proved to be a more effective catalyst with approximately 43% of the substrate converted to six metabolites, including 20% conversion to the aliphatic carbinol **3** as a major route. CYP2D6 was less active (33% conversion), with aromatic hydroxylation to give **4** as the dominant pathway (27%). The Cl_{int} values at 1 μM were <0.2 μl/min/pmol P450 ($t_{1/2}$ >40 min) in both CYP2D6 and CYP3A4, indicating a low turnover for the compound in the two enzymes.

Identification of Levallorphan Metabolites. The product ion spectrum of protonated levallorphan (**2H⁺** at *m/z* 284.1986; see Supplemental Data Fig. S9) was essentially identical to that of protonated levorphanol (**1H⁺**) shown in Fig. 2. This behavior makes clear that collision-induced dissociation of **1H⁺** and **2H⁺** proceeds via the same two initial fragmentation reactions [(a) and (b)] shown for **1H⁺** in Scheme 1. The only unique product ions formed from **2H⁺** are the ring-opened ions **xxxa⁺** and **xxxb⁺** (Scheme 3) that replace **ia⁺** and **ib⁺** formed from **1H⁺**.

Incubations of Levallorphan with CYP3A4 and CYP2D6. The total ion current chromatograms (TICs) of incubation extracts ob-
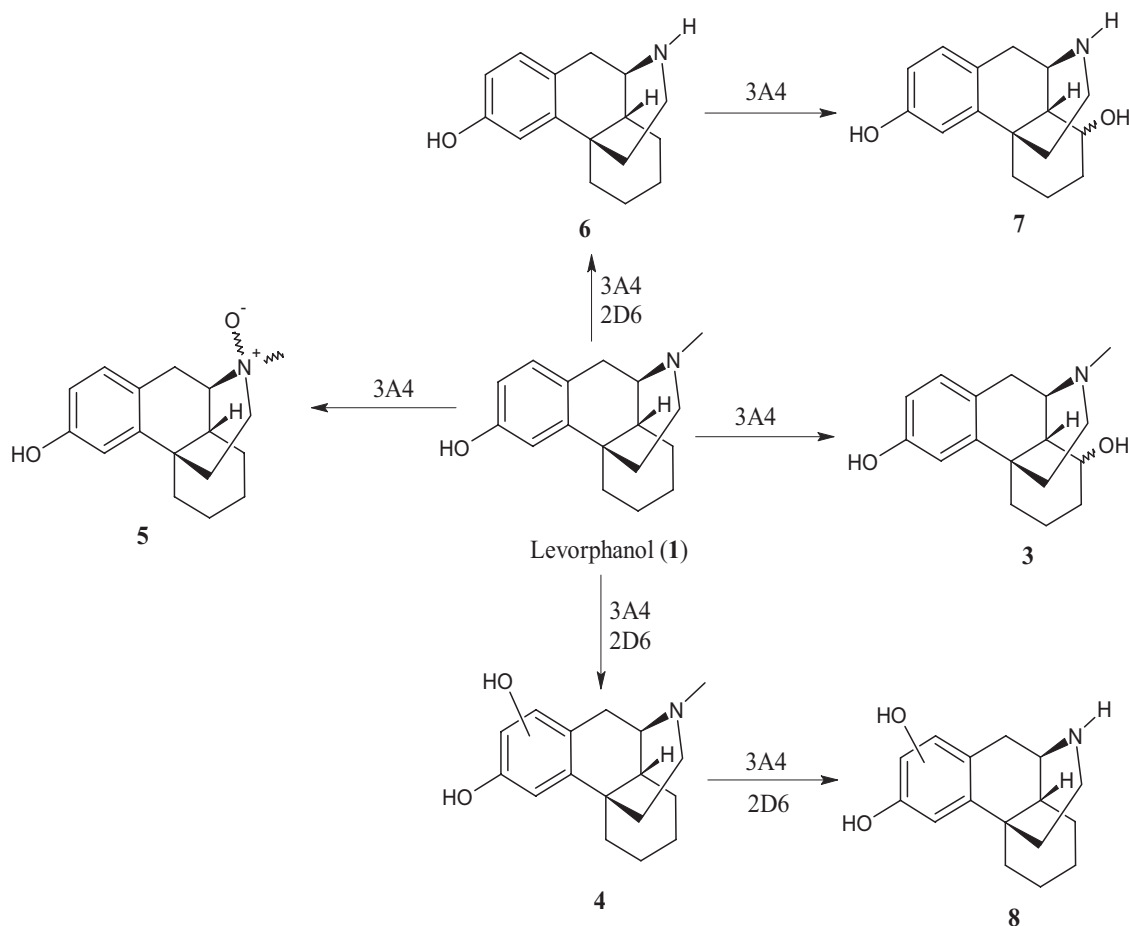
SCHEME 2. Proposal for the in vitro metabolic pathways of levorphanol (**1**) catalyzed by CYP3A4 and CYP2D6.

TABLE 3

MS response areas and %MS of levorphanol, levallorphan, and the observed metabolites after 60-min incubations with recombinant CYP2D6 and CYP3A4

Compound	MS Response Area (10^7 cps)		%MS[a]	
	3A4	2D6	3A4	2D6
Levorphanol (**1**)	7.40	7.91	57	67
3	2.54	3.15	20	
4	0.40		3.1	27
5	0.77	0.41	6	
6	0.72	0.41	5.6	3.4
7	0.16		1.2	
8	0.39	0.38	3.1	3.2
Levallorphan (**2**)	5.59	7.71	39	84
6	1.90	0.299	13	3.2
9	2.41		17	
10	1.29	0.240	9	2.6
11	0.819	0.52	5.7	5.6
12	0.53		3.7	
13	0.417		2.9	

[a] %MS calculated from MS response area divided by the summed areas of all the metabolites and parent.

tained with levallorphan (**2**) in the presence of CYP3A4 revealed six metabolite peaks; the corresponding chromatograms with CYP2D6 showed only three metabolite peaks, all of which were present in the CYP3A4 tracing. The XICs of these analytes are shown in Fig. 4.

The retention time and product ion spectra of the CYP3A4- and CYP2D6-generated species observed at *m/z* 244 were identical to those of the *N*-demethylated metabolite **6** of levorphanol. Consequently, this compound must be the *N*-deallylated metabolite of levallorphan (**6**, Scheme 4). The other five levallorphan metabolites were identified as **9** through **13** (see below). In addition to **6**, compounds **10** and **11** were common metabolites of CYP3A4 and CYP2D6. The ions obtained from the product ion spectra are reported in Table 2.
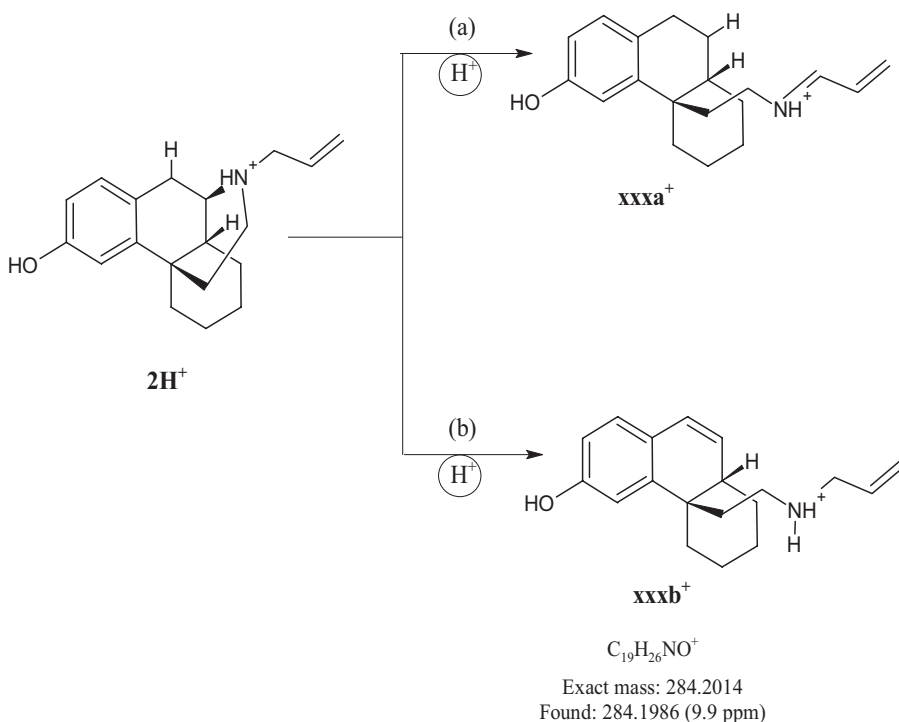
A summary of the metabolic pathways of levallorphan including structures of metabolites is depicted in Scheme 4. Metabolites **9** and **10** have MH$^+$ at *m/z* 300.1934/300.1955, 16 *m/z* units greater than

that of levallorphan, suggesting formation of hydroxylated metabolites. The structure proposed for **9** is the C(5)-cyclohexylcarbinol (**9**, Scheme 4). This assignment is based on the same analysis that led to the assignment of **3** for the levorphanol metabolite because the product ions of **9H$^+$** correspond to the product ions observed for **3H$^+$**. In particular, the loss of 18 *m/z* units (water) to give *m/z* 282.1799 supports the proposed aliphatic hydroxylation site. The product ion spectrum of the second + 16 metabolite displays ions corresponding to those observed for **4**, the aromatic hydroxylated metabolite of levorphanol. That leads to structure **10** for this metabolite (Scheme 4).

Compounds assigned structures **11** and **12** (MH$^+$ at *m/z* 316.1920) have a mass difference compared with levallorphan of +32 *m/z* units, indicating *bis*-hydroxylations. The MS^2-generated product ions of **11** correspond to the product ions observed with the carbinol metabolite **9** of levallorphan except for the increase of 16 Da for the second hydroxyl group. The presence of a product ion at *m/z* 161.0612 in the MS^2 of **11**, corresponding to **v$^+$** (see Supplemental Data Scheme S2) with the addition of 16 *m/z* units, suggests that the second hydroxylation is positioned in the aromatic ring [C(10) or C(13)] (**11**, Scheme 4). The proposed structure of **12** is shown in Scheme 4. This compound is also a *bis*-hydroxylated metabolite of levallorphan that, in this case, seems to involve two oxidations of the cyclohexyl ring (ring C). This conclusion is based on comparisons of the product ions present in the MS^2 tracing of **12** with those formed in the MS^2 of **9** and **10** (see Supplemental Data Scheme S7 for details).

The compound assigned structure **13** has MH$^+$ at *m/z* 258.1472, 26 *m/z* units less than the parent **2H$^+$**. This mass corresponds to *N*-deallylation and hydroxylation of the parent followed by further oxidation of a carbinol group to a carbonyl group. The MS^2 fragmentation pattern differs from those of other compounds in the series. This leads to the suggestion that the carbonyl group is positioned α to the nitrogen atom resulting in the lactam **13** (Scheme 4). This proposal is supported by the observed product ions that are discussed in detail in the supplemental data (Scheme S8).

In addition to the aforementioned metabolites, three weak signals were observed at *m/z* 314 (data not shown). The mass difference of 30

(a)
H$^+$
xxxa$^+$

(b)
H$^+$
xxxb$^+$

2H$^+$

C$_{19}$H$_{26}$NO$^+$
Exact mass: 284.2014
Found: 284.1986 (9.9 ppm)

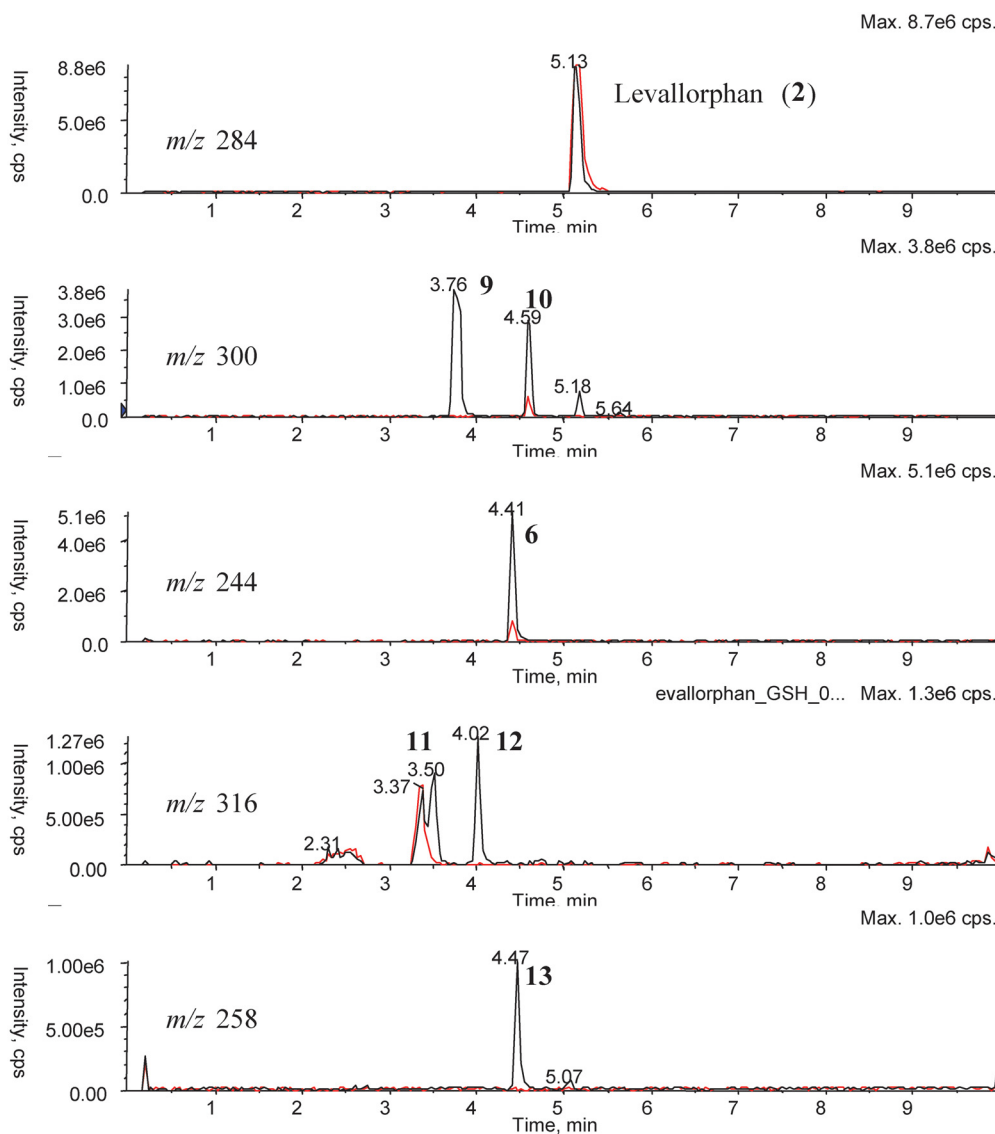SCHEME 3. Formation of product ions **xxxa$^+$** and **xxxb$^+$** from **2H$^+$**.

FIG. 4. XICs obtained from extracts of incubation mixtures of levallorphan (10 μM) in the presence of NADPH-supplemented recombinant CYP3A4 (black) and CYP2D6 (red).

m/z units compared with the parent compound suggests double hydroxylations and further oxidation to a carbonyl group. No structural assignments are offered for these three secondary metabolites.

The absolute MS response area for each metabolite of levallorphan together with the %MS are presented in Table 3. The main species detected in the HPLC/MS analysis is the parent drug, particularly in the CYP2D6 incubations. Based on the %MS, the major metabolite formed with CYP3A4 results from hydroxylation in the cyclohexyl ring. The three CYP2D6-generated metabolites appear to be formed in approximately equal amounts. The Cl_{int} values at 1 μM were <0.2 μl/min/pmol P450 ($t_{1/2}$ >40 min) in CYP2D6 and 0.82 μl/min/pmol P450 ($t_{1/2}$ 8.5 min) in CYP3A4, indicating a higher turnover for levallorphan in CYP3A4.

IC_{50} Determinations. To determine the reversible inhibition potentials of levorphanol (**1**) and levallorphan (**2**) on CYP3A4 and CYP2D6, full IC_{50} curves were obtained. The IC_{50} values for levorphanol were >50 μM in the CYP3A4 assay and 11.5 μM in the CYP2D6 assay. The corresponding values for levallorphan were >50 μM in the CYP3A4 assay and 0.65 μM in the CYP2D6 assay. These results indicate that both compounds act as relatively strong reversible inhibitors of CYP2D6, but neither of them shows any inhibition of CYP3A4.

Time-Dependent Inhibition. The two test compounds also were analyzed for their potential TDI properties. After preincubation with each test compound in the presence and absence of NADPH, the enzyme activity was measured in incubations with the probe substrates AMMC (CYP2D6) and BFC (CYP3A4). The results for levallorphan showed a decrease in CYP2D6 activity at higher concentrations both in samples preincubated with and without NADPH. This result suggests that levallorphan is a strong, reversible inhibitor. No changes were obtained with the 1/20 dilution compared with the results from the 1/10 dilution that are reported here. From the results of levallorphan incubated with CYP2D6, a concentration-dependent loss of activity was observed but it was not time-dependent. To diminish this time-independent component the activity was normalized to the incubations carried out in the absence of NADPH. The normalized ratios (NRs) were calculated according to the following equation:

$$NR = \frac{(A_{inh}/A_{ctrl})}{(A_{inh}/A_{ctrl})_{wo\ NADPH}}$$

where A_{inh} is the catalytic activity after preincubation with inhibitor present and A_{ctrl} is the activity in the control incubations without inhibitor. A compound is considered to be a time-dependent inhibitor
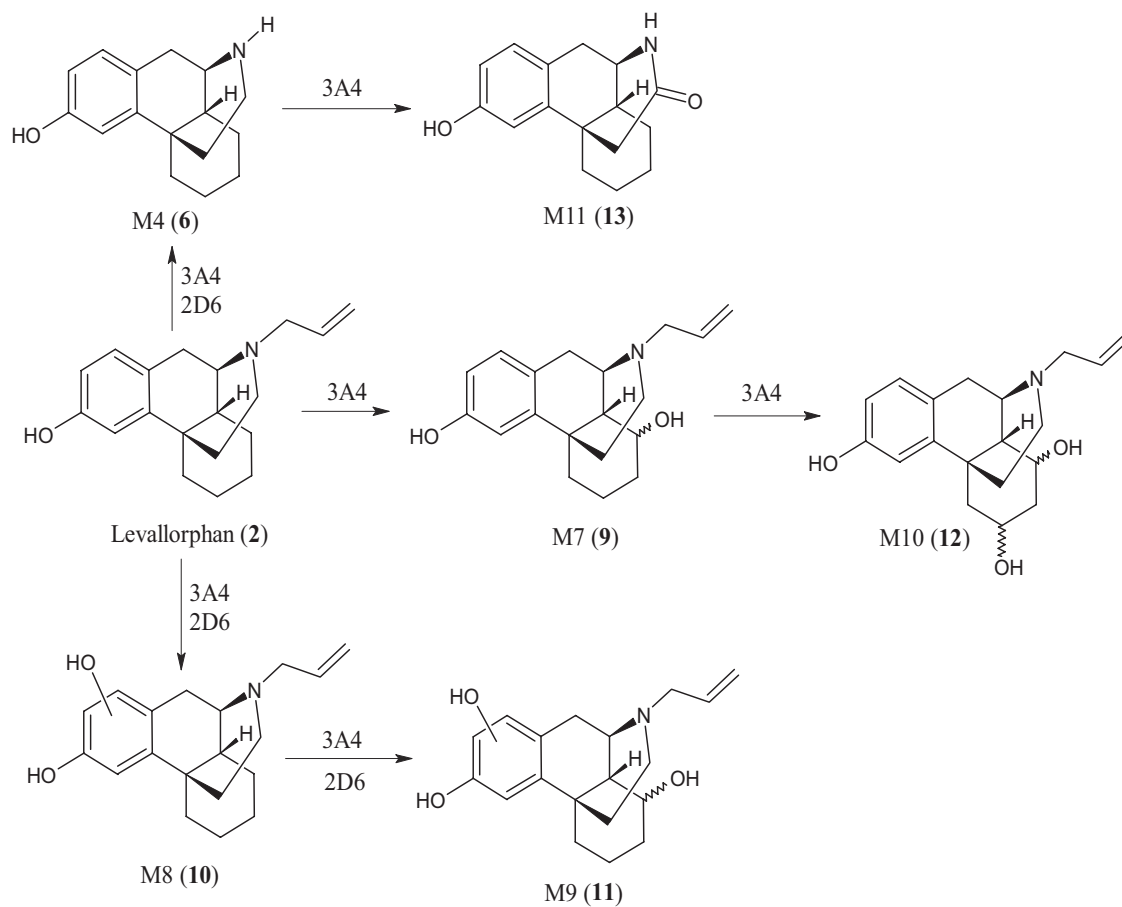
SCHEME 4. Proposed in vitro metabolic pathways of levallorphan (2) catalyzed by CYP2D6 and CYP3A4.

if the NR is less than 0.7. This is an empirical value based on the understanding that the value for a compound not acting as a time-dependent inhibitor should be approximately 1.0. Allowing for an experimental error of 20%, it could be higher or lower. Hence there is a gray zone for NR = 0.7 to 0.9.

The NRs for the two test compounds, after 20 min of preincubations, together with those of the positive controls, are presented in Fig. 5. Complete time curves are presented in the Supplemental Data Figs. S17 and S18. From the NR values it was apparent that levallorphan acts as a time-dependent inhibitor on CYP3A4 (NR 0.45 at 12.5 μM and NR 0.27 at 25 μM) but not on CYP2D6. Levorphanol, which lacks the allylic side chain, did not act as a time-dependent inhibitor on either CYP3A4 or CYP2D6.

It is noteworthy that levallorphan shows strong reversible inhibition (IC$_{50}$ = 0.65 μM) but no TDI of CYP2D6. The opposite results observed with CYP3A4 could indicate differences in how the two isoenzymes interact with this substrate. The difference in the TDI properties with CYP3A4 for levallorphan and levorphanol supports the involvement of the allylic side chain of levallorphan in the mediation of the observed TDI.

Studies with Glutathione. The presence of the allylic side chain in levallorphan and the fact that this compound acts as a time-dependent inhibitor of CYP3A4 led to glutathione trapping studies that were designed to trap possible metabolically generated reactive species. The result could indicate a possible relationship between the TDI and the anticipated bioactivation of levallorphan to reactive species.

TICs obtained with levallorphan incubations in the presence of GSH and CYP3A4 or CYP2D6 are presented in Fig. 6. In MS^2 tracings of the CYP3A4 incubations, a large peak with the retention time 4.18 min at m/z 589 was observed. This mass corresponds to the

mass of **2** + 307 − H$_2$ + H$^+$, consistent with a glutathionyl conjugate of levallorphan that had undergone an initial 2-electron (net loss of H$_2$) oxidation (Scheme 5). The suggested structure, **16**, reflects the proposed 1,4-addition reaction of GSH with the eneiminiumyl metabolite **15$^+$** formed by initial oxidation (hydroxylation followed by dehydration of the protonated carbinol **14H$^+$** oxygen atom) of the carbon atom α to the nitrogen atom of levallorphan. Less likely would be 1,2-addition because the terminal carbon atom of the eneiminiumyl moiety is sterically less hindered than the internal π-bond. In addition, the proposed 1,4-addition product **16** will be more stable than the corresponding 1,2-addition product because of the conjugation of the nitrogen lone pair with the π-bond. The principal fragment ion observed in the MS^2 of MH$^+$ at m/z 589 was at m/z 282 as expected because the glutathionyl group is in conjugation with the eneaminyl system and should readily eliminate following protonation of sulfur to give the eneiminiumyl fragment (m/z 282) with glutathione as the neutral loss (Scheme 6). The second diagnostic fragment ion observed at m/z 460 corresponds to the expected neutral loss of pyroglutamic (129 Da) that is characteristic of glutathionyl adducts (see Supplemental Data Scheme S9 for details).

In addition to **16H$^+$** two minor peaks at 0.7 and 5.14 min are present in both the CYP3A4 and CYP2D6 incubations. These peaks have MH$^+$ at m/z 605, corresponding to a glutathionyl conjugate of hydroxylated levallorphan (**2** + 305 + 16 + H$^+$). The MS^2 tracings of these peaks were weak, and no structural assignments were attempted. Possible metabolites could result from epoxidation of either the allyl or the aromatic moiety followed by conjugation with GSH. These peaks are considered to be minor metabolites and are not considered further.
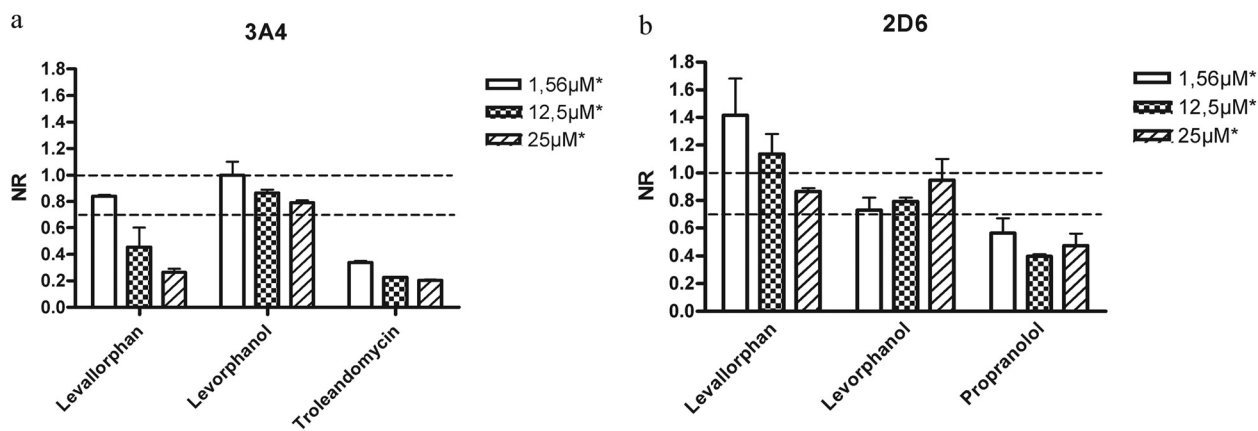
FIG. 5. Normalized ratios from the TDI assay with CYP3A4 (a) and CYP2D6 (b). The values are averages of data obtained from two incubations with the S.D. represented by error bars. The area between the dotted lines is considered to be a gray zone (see definition under *Results*). ∗ for troleandomycin the corresponding concentrations used were 0.3, 2.5, and 5 μM. For propranolol the concentrations used were 0.6, 5, and 10 μM.
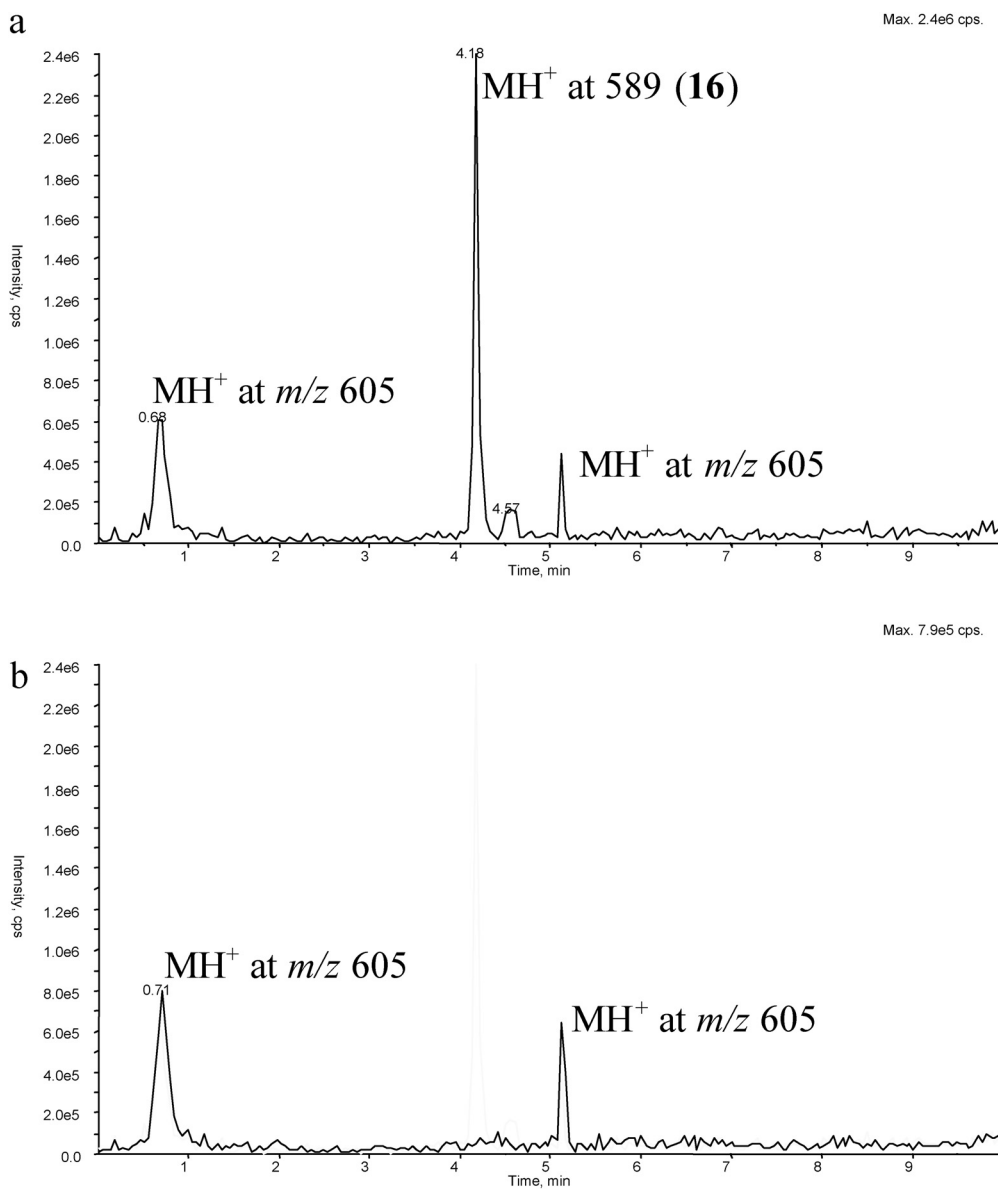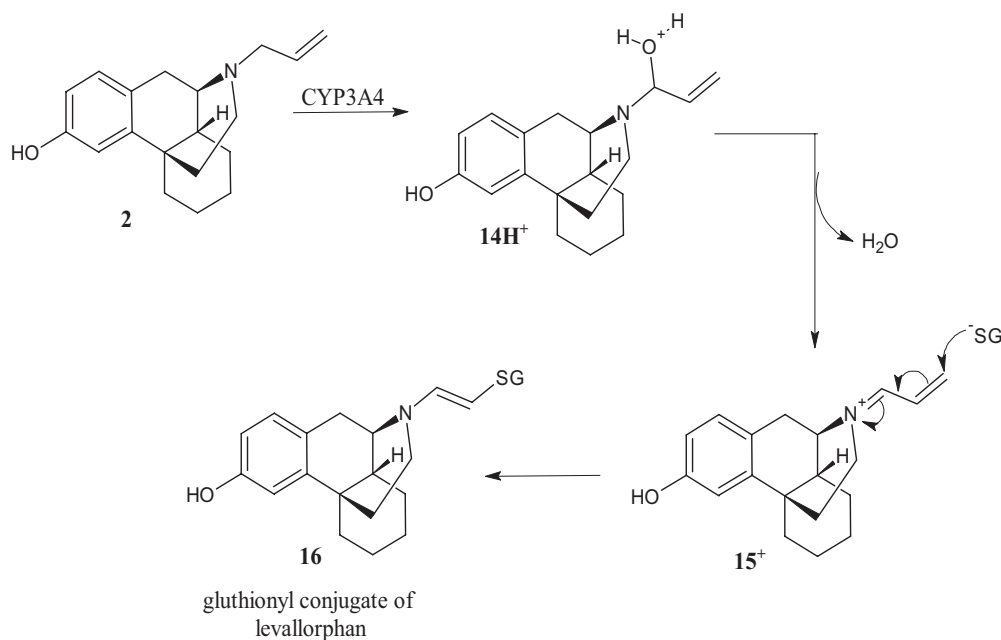

FIG. 6. TIC from the HPLC/MS experiment of the incubation mixture of levallorphan (10 μM) supplemented with NADPH and GSH with recombinant CYP3A4 (a) and recombinant CYP2D6 (b).

SCHEME 5. Proposed mechanism for the formation of the glutathionyl conjugate **16** of levallorphan.

gluthionyl conjugate of levallorphan

Dockings of Levorphanol and Levallorphan into Crystal Structures of CYP2D6 and CYP3A4. In CYP2D6 three poses each of levorphanol and levallorphan were obtained. Comparing the calculated interaction energies, two poses are indicated to be the most favorable. These are presented in Fig. 7, a and b, and represent an orientation of levallorphan and levorphanol with the aromatic ring/phenol toward the heme. For levallorphan the distance between the positively charged nitrogen and the negatively charged Glu216 was 4.64 Å, and the distance to the oxy species in the heme was 3.55 Å. For levorphanol these distances were 7.50 and 2.87 Å, respectively. The other two poses of levallorphan were with the allyl group pointing toward the heme, and an additional pose is with the aromatic moiety toward the heme. Levorphanol also showed an additional pose with the aromatic ring closest to the heme and one with the pyridine ring pointing toward the heme. Docking energies and information about the orientation of each docking pose are available in the Supplemental Data Table S1.

In contrast to the limited number of docking poses in CYP2D6, the dockings in CYP3A4 revealed 19 poses of levallorphan and levorphanol. The calculated interaction energies did not differ much between these poses, and there was no obvious ranking among them. The poses represent orientations of the substrates presenting many different parts of the molecule to the heme. Some examples are visualized in Fig. 8. In general, most of the levallorphan poses were far away from the heme compared with levorphanol. These poses might be favored by hydrophobic interactions with the phenyl alanine cluster in CYP3A4. Docking energies and information about the

orientation of each docking pose are available in the Supplemental Data Table S1.

Interaction energies between each docking pose and the surrounding amino acid residues were calculated with the energy calculation method described previously (Kjellander et al., 2007). These data are available in Supplemental Data Tables S2 and S3.

Discussion

The rationales for the present study included the possibility of exploring orientations of the two selected compounds, levallorphan and levorphanol, in the active sites of CYP2D6 versus CYP3A4 in vitro and in silico. Our approach involved metabolic profiling studies on levallorphan and levorphanol with the key tool being the characterization of metabolites using recombinant enzymes. The inhibition potentials of levallorphan and levorphanol on CYP2D6 and CYP3A4 were also examined in an effort to assess their affinities for these enzymes. In addition, their TDI properties were explored in part because of the presence of the allylic side chain in levallorphan, a structural feature often associated with TDI (Fontana et al., 2005). We anticipated that the results of these experiments would provide useful insights into how these compounds would be oriented in the enzyme active site cavities of the two P450 isoforms to give productive binding modes. Finally, glutathionyl trapping experiments were performed on levallorphan to determine whether the formation of glutathionyl conjugates correlated with the observed TDI of this allylamine derivative.

CYP2D6 catalyzed only the aromatic hydroxylation and *N*-demethylation/*N*-deallylation pathways, consistent with an orientation of the
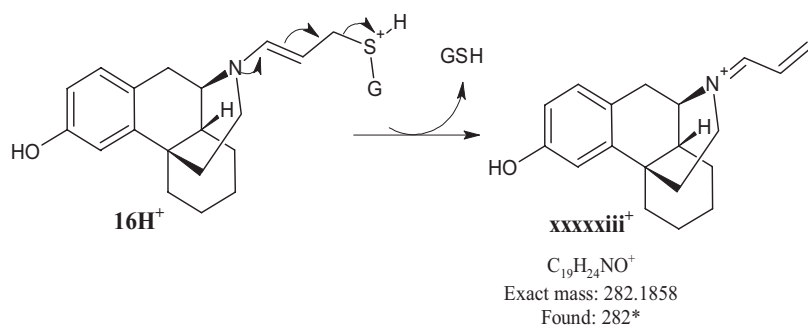
SCHEME 6. Proposed mechanism to account for the observed fragment **xxxxxiii**[+] in the MS[2] of **16H**[+]. * no accurate mass available for the GSH adduct and its product ion.

$C_{19}H_{24}NO^{+}$
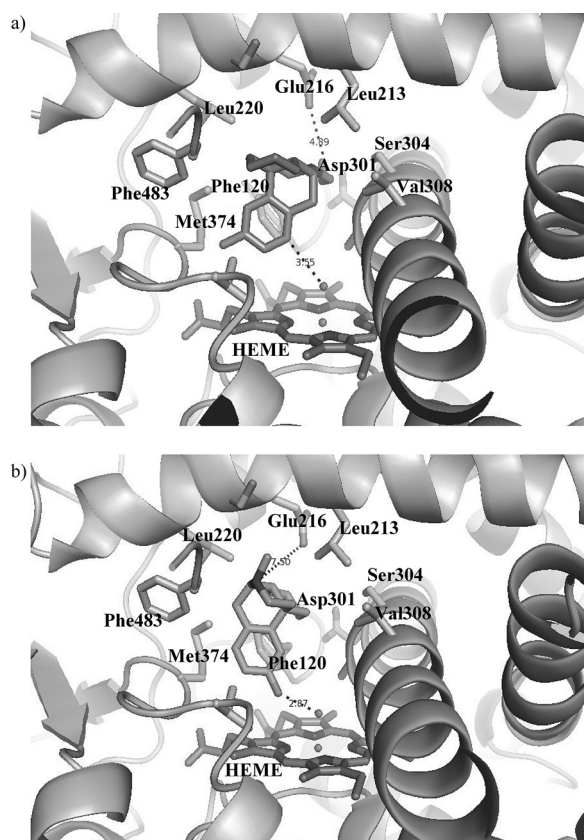Exact mass: 282.1858
Found: 282*

FIG. 7. Levallorphan (a) and levorphanol (b) docked in active site cavity of CYP2D6 crystal structure (Protein Data Bank code 2f9q).
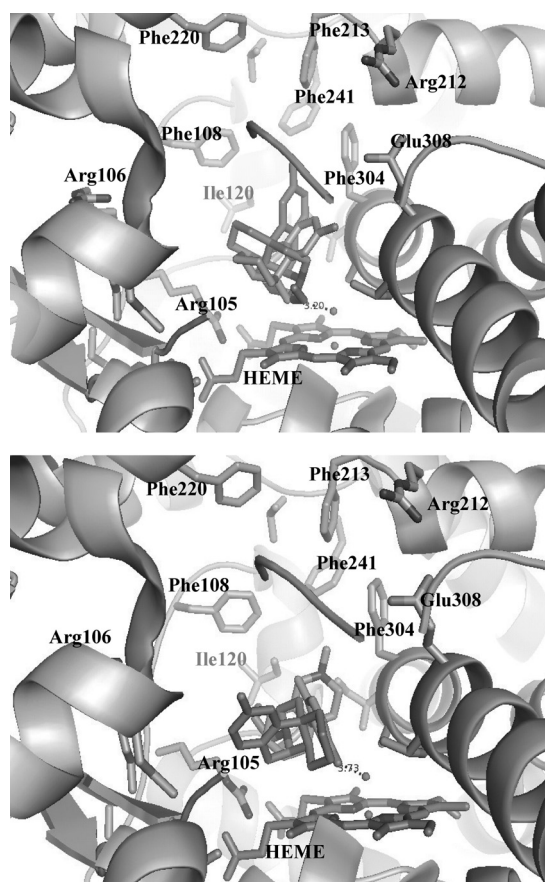

FIG. 8. Levallorphan and levorphanol docked in active site cavity of CYP3A4 crystal structure (Protein Data Bank code 2j0d).

substrate with the aromatic moiety or the nitrogen atom pointing toward the heme. These orientations were also those obtained from the docking experiments. The orientation with the aromatic moiety toward the heme was the most favorable with respect to calculated interaction energies. The CYP2D6 substrate/inhibitor pharmacophore is proposed to consist of interactions with a basic nitrogen atom of the substrate and acidic amino acid residues of the enzyme (Glu216 and Asp301) that fix the substrate at a defined distance from the site of metabolism. In addition, a hydrophobic region is suggested to be present near the site of oxidation. Site-directed mutagenesis studies have documented the influence of the hydrophobic amino acids, Phe120 and Phe483, on the regioselectivity of some CYP2D6 substrates (Flanagan et al., 2004; Lussenburg et al., 2005). The importance of the interactions between the basic nitrogen and acidic amino acid residues in the active site also have been supported by site-directed mutagenesis studies (Guengerich et al., 2003; Paine et al., 2003). In addition, Upthagrove and Nelson (2001) have shown a relationship between substrate affinity and pK_a of the substrate. From this knowledge of CYP2D6 and its substrates it could be hypothesized that an orientation of the ligand with the nitrogen pointing away from the heme is favored, and consequently N-dealkylation is unlikely to occur. The orientation with the aromatic ring in levorphanol/levallorphan toward the heme is consistent with the proposed CYP2D6 pharmacophore, whereas the orientation with the nitrogen toward the heme does not fit this analysis. However, considering the amount of metabolites formed, the N-dealkylation is only a minor pathway in CYP2D6. In the best pose obtained from the dockings of levallorphan the basic nitrogen is 4.6 Å from the Glu216. In addition, Phe120 seems to interact with the hydrophobic core structure of the ligand. For levorphanol a similar picture is obtained, but the nitrogen in the

ligand is rather far away from the acidic amino acid residue in the active site. However, this picture is a static view of the protein, and in reality the side chains of the amino acids are flexible and are allowed to move in the active site.

Comparing the extent of metabolism of levorphanol and levallorphan with the selected isoenzymes made clear that both compounds were more extensively metabolized by CYP3A4 than CYP2D6. The CYP3A4 metabolites observed indicated that both compounds could be oriented in different ways in the active site, resulting in the presentation of different regions of the molecule to the heme. CYP3A4 has a larger and flexible active site in which hydrophobic interactions with the ligand will probably dominate (see Fig. 8). In contrast to CYP2D6, N-dealkylation reactions are more common with CYP3A4 as a result of an orientation with the nitrogen atom in the ligand oriented toward the heme (Coutts et al., 1994). These results also are consistent with the large number of energetically expectable docking solutions obtained with CYP3A4.

Besides metabolic profiling of compounds in different P450s, the inhibition potentials of the compounds are of interest. P450 inhibition can result from a nonproductive binding mode of a substrate and may give an indication of the orientation in the active site. The potential to inhibit CYP2D6 and CYP3A4 in a reversible manner was determined for levorphanol and levallorphan. From the resulting IC_{50} values neither of the two compounds proved to inhibit CYP3A4. On the other hand, both compounds inhibited CYP2D6. If applying the CYP2D6 substrate/inhibitor pharmacophore to the interactions of these two compounds, the preferred orientation would be with the oxygen atom of the aromatic moiety pointing toward the heme and the nitrogen atom pointing away from the heme. Interactions between the basic

nitrogen atom and the acidic amino acid residues in the active site cavity may favor a nonproductive orientation of the substrate that could, in theory, result in enzyme inhibition. From the dockings, however, it is difficult to draw any conclusions about the inhibitory or productive binding modes of the ligands. In this case the high affinity of levallorphan for CYP2D6, reflected by its low IC_{50} value, might be the result of hydrophobic interactions between the allyl chain and the protein, as well as electrostatic interactions with the acidic amino acids. In CYP3A4, on the other hand, both compounds were extensively metabolized but did not inhibit the substrate in a reversible manner. This result is clearly consistent with the different character of the active sites of CYP2D6 and CYP3A4 as discussed above.

The potential TDI properties of levallorphan and levorphanol also were examined. As anticipated, levorphanol, which lacks the allylic side chain, did not show any TDI properties, whereas the allylaminyl substrate levallorphan proved to be a time-dependent inhibitor. A difference in the TDI properties of levallorphan with the two isoenzymes should give an indication of binding modes in CYP2D6 and CYP3A4 because the assay reports on the TDI properties of the test compound that presumably involve the formation of reactive species. That is, a metabolite is formed that in turn can form adducts with the protein. The mechanism of inactivation is not considered here, only the formation of the reactive metabolite. Studies on the TDI properties established that levallorphan inactivated CYP3A4 but not CYP2D6, suggesting that a reactive species is formed in the presence of CYP3A4 but not in the presence of CYP2D6. From the glutathionyl trapping experiment a large peak, corresponding to a glutathionyl adduct (**16**) at the allylic side chain of levallorphan, was present in incubations with CYP3A4. The suggested adduct position of the glutathionyl moiety is consistent with that previously reported in the literature for allylamines that cause time-dependent inactivation of P450 (Fontana et al., 2005). The absence of any large peak corresponding to a glutathionyl adduct of levallorphan in CYP2D6 incubations correlates with the lack of TDI properties of levallorphan on this enzyme. This is in agreement with the discussion that the environment in the active site cavity of CYP2D6 orients the ligands with the basic nitrogen pointing away from the heme.

In summary, studies of the metabolism and inhibition potentials of levorphanol and levallorphan with CYP2D6 and CYP3A4 have led to information on how these compounds interact with these two isoenzymes of P450. Rationalizations of the fragmentation pathways observed in the product ion spectra for the metabolites formed from levorphanol and levallorphan have provided an opportunity to characterize the orientations of these molecules in the respective enzyme active sites. From the metabolites formed it may be concluded that substrates may have several productive orientations in the active site of CYP3A4. In CYP2D6, on the other hand, the compounds orient with the aromatic moiety or the nitrogen atom pointing toward the heme. The *N*-dealkylated metabolites, not following the CYP2D6 pharmacophore, were only minor compared with those formed in CYP3A4. Furthermore, the TDI properties observed with levallorphan and the formation of a glutathionyl conjugate of this compound with CYP3A4 but not with CYP2D6 strongly indicate that levallorphan adopts a productive binding mode in CYP3A4 that is not allowed in CYP2D6. These results support the hypothesis that the acidic amino acid residues in the CYP2D6 active site cavity favor an orientation of the substrate with the nitrogen pointing away from the heme, whereas orientations with the nitrogen atom toward the heme are commonly observed in CYP3A4. These results are also consistent with the dockings and support previous conclusions reached from computational studies of the enzymes in which CYP3A4 is suggested to have a more flexible active site with hydrophobic interactions as major determinants for ligand-enzyme affinity, whereas CYP2D6 has a more restricted active site with electrostatic interactions with the ligand as an important factor.

References

Benetton SA, Borges VM, Chang TK, and McErlane KM (2004) Role of individual human cytochrome P450 enzymes in the in vitro metabolism of hydromorphone. *Xenobiotica* **34:**335–344.

Coutts RT, Su P, and Baker GB (1994) Involvement of CYP2D6, CYP3A4, and other cytochrome P-450 isozymes in N-dealkylation reactions. *J Pharmacol Toxicol Methods* **31:**177–186.

de Groot MJ, Bijloo GJ, Martens BJ, van Acker FA, and Vermeulen NP (1997) A refined substrate model for human cytochrome P450 2D6. *Chem Res Toxicol* **10:**41–48.

De Rienzo F, Fanelli F, Menziani MC, and De Benedetti PG (2000) Theoretical investigation of substrate specificity for cytochromes P450 IA2, P450 IID6 and P450 IIIA4. *J Comput Aided Mol Des* **14:**93–116.

Ekroos M and Sjögren T (2006) Structural basis for ligand promiscuity in cytochrome P450 3A4. *Proc Natl Acad Sci U S A* **103:**13682–13687.

Flanagan JU, Maréchal JD, Ward R, Kemp CA, McLaughlin LA, Sutcliffe MJ, Roberts GC, Paine MJ, and Wolf CR (2004) Phe120 contributes to the regiospecificity of cytochrome P450 2D6: mutation leads to the formation of a novel dextromethorphan metabolite. *Biochem J* **380:**353–360.

Fontana E, Dansette PM, and Poli SM (2005) Cytochrome p450 enzymes mechanism based inhibitors: common sub-structures and reactivity. *Curr Drug Metab* **6:**413–454.

Goodford PJ (1985) A computational procedure for determining energetically favorable binding sites on biologically important macromolecules. *J Med Chem* **28:**849–857.

Guengerich FP (2003) Cytochromes P450, drugs, and diseases. *Mol Interv* **3:**194–204.

Guengerich FP, Hanna IH, Martin MV, and Gillam EM (2003) Role of glutamic acid 216 in cytochrome P450 2D6 substrate binding and catalysis. *Biochemistry* **42:**1245–1253.

Hutchinson MR, Menelaou A, Foster DJ, Coller JK, and Somogyi AA (2004) CYP2D6 and CYP3A4 involvement in the primary oxidative metabolism of hydrocodone by human liver microsomes. *Br J Clin Pharmacol* **57:**287–297.

Kirkwood LC, Nation RL, and Somogyi AA (1997) Characterization of the human cytochrome P450 enzymes involved in the metabolism of dihydrocodeine. *Br J Clin Pharmacol* **44:**549–555.

Kjellander B, Masimirembwa CM, and Zamora I (2007) Exploration of enzyme-ligand interactions in CYP2D6 & 3A4 homology models and crystal structures using a novel computational approach. *J Chem Inf Model* **47:**1234–1247.

Koymans L, Vermeulen NP, van Acker SA, te Koppele JM, Heykants JJ, Lavrijsen K, Meuldermans W, and Donné-Op den Kelder GM (1992) A predictive model for substrates of cytochrome P450-debrisoquine (2D6). *Chem Res Toxicol* **5:**211–219.

Lewis DF (1999) Homology modelling of human cytochromes P450 involved in xenobiotic metabolism and rationalization of substrate selectivity. *Exp Toxicol Pathol* **51:**369–374.

Lewis DF, Eddershaw PJ, Goldfarb PS, and Tarbit MH (1997) Molecular modelling of cytochrome P4502D6 (CYP2D6) based on an alignment with CYP102: structural studies on specific CYP2D6 substrate metabolism. *Xenobiotica* **27:**319–339.

Lussenburg BM, Keizers PH, de Graaf C, Hidestrand M, Ingelman-Sundberg M, Vermeulen NP, and Commandeur JN (2005) The role of phenylalanine 483 in cytochrome P450 2D6 is strongly substrate dependent. *Biochem Pharmacol* **70:**1253–1261.

Narimatsu S, Arai T, Masubuchi Y, Horie T, Hosokawa M, Ueno K, Kataoka H, Yamamoto S, Ishikawa T, and Cho AK (2001) Inactivation of rat cytochrome P450 2D enzyme by a further metabolite of 4-hydroxypropranolol, the major and active metabolite of propranolol. *Biol Pharm Bull* **24:**988–994.

Paine MJ, McLaughlin LA, Flanagan JU, Kemp CA, Roberts GC, and Wolf CR (2003) Residues glutamate 216 and aspartate 301 are key determinants of substrate specificity and product regioselectivity in cytochrome P450 2D6. *J Biol Chem* **278:**4021–4027.

Poulos TL, Finzel BC, and Howard AJ (1987) High-resolution crystal structure of cytochrome P450cam. *J Mol Biol* **195:**687–700.

Rowland P, Blaney FE, Smyth MG, Jones JJ, Leydon VR, Oxbrow AK, Lewis CJ, Tennant MG, Modi S, Eggleston DS, et al. (2006) Crystal structure of human cytochrome P450 2D6. *J Biol Chem* **281:**7614–7622.

von Moltke LL, Greenblatt DJ, Grassi JM, Granda BW, Venkatakrishnan K, Schmider J, Harmatz JS, and Shader RI (1998) Multiple human cytochromes contribute to biotransformation of dextromethorphan in-vitro: role of CYP2C9, CYP2C19, CYP2D6, and CYP3A. *J Pharm Pharmacol* **50:**997–1004.

Williams PA, Cosme J, Vinkovic DM, Ward A, Angove HC, Day PJ, Vonrhein C, Tickle IJ, and Jhoti H (2004) Crystal structures of human cytochrome P450 3A4 bound to metyrapone and progesterone. *Science* **305:**683–686.

Yamazaki H and Shimada T (1998) Comparative studies of in vitro inhibition of cytochrome P450 3A4-dependent testosterone 6beta-hydroxylation by roxithromycin and its metabolites, troleandomycin, and erythromycin. *Drug Metab Dispos* **26:**1053–1057.

Yano JK, Wester MR, Schoch GA, Griffin KJ, Stout CD, and Johnson EF (2004) The structure of human microsomal cytochrome P450 3A4 determined by X-ray crystallography to 2.05-A resolution. *J Biol Chem* **279:**38091–38094.

Yue QY and Säwe J (1997) Different effects of inhibitors on the O- and N-demethylation of codeine in human liver microsomes. *Eur J Clin Pharmacol* **52:**41–47.

Address correspondence to: Britta Bonn, Discovery DMPK, AstraZeneca R&D Mölndal, SE-43181 Mölndal, Sweden. E-mail: kjelland@chem.gu.se